



HAL
open science

Ultrafast demagnetization in buried Co₈₀Dy₂₀ as fingerprint of hot-electron transport

T. Ferté, N. Bergéard, G. Malinowski, E. Terrier, L. Le Guyader, K. Holldack, M. Hehn, C. Boeglin

► To cite this version:

T. Ferté, N. Bergéard, G. Malinowski, E. Terrier, L. Le Guyader, et al.. Ultrafast demagnetization in buried Co₈₀Dy₂₀ as fingerprint of hot-electron transport. *Journal of Magnetism and Magnetic Materials*, 2019, 485, pp.320-324. <10.1016/j.jmmm.2019.04.068>. <hal-02339472>

HAL Id: hal-02339472

<https://hal.science/hal-02339472v1>

Submitted on 22 Oct 2021

HAL is a multi-disciplinary open access archive for the deposit and dissemination of scientific research documents, whether they are published or not. The documents may come from teaching and research institutions in France or abroad, or from public or private research centers.

L'archive ouverte pluridisciplinaire HAL, est destinée au dépôt et à la diffusion de documents scientifiques de niveau recherche, publiés ou non, émanant des établissements d'enseignement et de recherche français ou étrangers, des laboratoires publics ou privés.



Distributed under a Creative Commons CC BY-NC 4.0 - Attribution - Non-commercial use - International License

1 Title: **Ultrafast demagnetization in buried Co₈₀Dy₂₀ as fingerprint of hot-electron**
2 **transport**

3
4 T. Ferté¹, N. Bergeard^{1*}, G. Malinowski², E. Terrier¹, L. Le Guyader³, K. Holldack³, M. Hehn²
5 and C. Boeglin¹

6 ¹ *Université de Strasbourg, CNRS, Institut de Physique et Chimie des Matériaux de*
7 *Strasbourg, UMR 7504, F-67000 Strasbourg, France.*

8 ² *Institut Jean Lamour, CNRS UMR 7198, Université de Lorraine, 54506 Vandoeuvre-lès-*
9 *Nancy, France.*

10 ³ *Institut für Methoden und Instrumentierung der Forschung mit Synchrotronstrahlung*
11 *Helmholtz-Zentrum Berlin für Materialien und Energie GmbH, Albert-Einstein-Str. 15, 12489*
12 *Berlin, Germany*

13
14 * Corresponding author:

15 *Mel: nicolas.bergeard@ipcms.unistra.fr*

16 *Address: Institut de Physique et de Chimie des Matériaux de Strasbourg (IPCMS)*

17 *Campus Cronenbourg 23 rue du Loess BP43 67034 Strasbourg*

18

19 **0. Abstract**

20

21 The generation of ultrashort hot-electron pulses in metallic heterostructures offers attractive
22 perspectives for the ultrafast spin manipulation on the picosecond time scale. In such
23 approach, the hot-electron pulses are produced by exciting a non-magnetic capping layer with
24 femtosecond infrared laser pulses. These hot-electron pulses propagate towards a buried
25 magnetic layer to trigger ultrafast demagnetization. Lately, it was shown that the
26 demagnetization onset and characteristic demagnetization times are both affected by the
27 transport regime (ballistic or diffusive) of the photo-excited hot-electrons. In this work, we
28 show that the hot-electron pulses produced by photo-exciting a Al(3)/Ta(3)/Cu(60) capping
29 layer undergo a temporal stretching and delays when they go across a [Co(0.1)/Ni(0.6)]_{x5}
30 multilayer. These information were extracted from a study of hot-electron induced
31 demagnetization in CoDy alloys by means of Time-Resolved X-Ray Magnetic Circular
32 Dichroism.

33 Key words:

34 Ultrafast demagnetization, Femtosecond laser, Hot-electron pulses, ferrimagnetic alloys

35

36 *1. Introduction*

37

38 Since the discovery of sub-picosecond demagnetization in Ni layers by femtosecond infrared
39 (IR) laser pulses [1], the quest towards ultrafast manipulation of spin in magnetic materials
40 has driven many experimental and theoretical investigations [2, 3, 4, 5]. In this context, the
41 All Optical Switching (AOS) of spins on the picosecond time scale induced by a single IR
42 laser pulse appeared as a major technological breakthrough for the data storage technologies
43 [6, 7]. However, this ultrafast reversal has been observed so far for a limited range of
44 materials such as FeCoGd alloys [8] and Co/Gd multilayers [9].

45 In recent years, sub-picosecond demagnetization induced by hot-electron pulses instead of IR
46 laser pulses was evidenced in a large variety of materials such as ferromagnetic transition
47 metal layers [10, 11], ferromagnetic alloys [12] or multilayers [13] and ferrimagnetic alloys
48 [14]. Subsequently, spin switching induced by a single hot-electron pulse was also
49 demonstrated in FeCoGd alloys [15]. In this alloy, the switching dynamics was shown to be as
50 fast as the reversal by a single IR pulse. In parallel, the ultrafast manipulation of spins in a
51 buried magnetic layer by using spin-polarized (SP) femtosecond hot-electron pulses has
52 triggered intensive researches in the field of “ultrafast spintronics” [16, 17, 18, 19, 20, 21].
53 The SP femtosecond hot-electron pulses can be generated by exciting a magnetic metal with
54 fs IR laser pulses. This has been theoretically predicted in the superdiffusive spin transport
55 model [22, 23] and evidenced in several experiments [24, 25, 26, 27, 28, 29]. For instance,
56 Alekhin et al. have produced SP hot-electron pulses by photo-exciting a thin Fe capping
57 deposited on a 100 nm thick Au layer to manipulate the magnetization in a buried Fe layer
58 [20]. In such geometry, the metallic capping layer is thicker than the typical IR laser
59 penetration depth to exclude parasitic laser excitations of the buried magnetic layer [30, 12].
60 Although hot-electron transport in the ballistic regime has been evidenced in thick noble
61 metals layers [31, 32], the actual spin polarization of hot-electrons transferred through tens of
62 nanometers in metals can be questioned. Indeed, Schellekens et al. evidenced a limited spin
63 diffusion length of such hot-electrons in Cu ($\lambda_{Cu} = 13\text{nm}$) [16]. This observation was recently
64 sustained by Iihama et al. [33].

65 An alternative route to generate and propagate highly SP hot-electron pulses towards a buried
66 magnetic layer consists in generating non polarized hot-electron in a metallic capping layer by
67 using IR laser pulses [5]. A thin magnetic layer is then inserted between the capping metallic

68 layer and the buried magnetic layer to polarize the hot-electrons via the spin-filtering effect
69 [34].

70 However, the insertion of a thin metallic layer in the path of the hot-electron pulses could
71 modify the electronic transport properties and subsequently change the magnetization
72 dynamics in the buried magnetic layer. For instance, we have shown that the insertion of a
73 Pt(10) layer between a Pt(3)/Cu(70) capping layer and a CoTb alloys was sufficient to
74 thermalize the photo-excited hot-electrons [14]. We also evidenced that although the
75 demagnetization induced by thermalized hot-electrons (with Pt(10)) is almost as efficient as
76 the demagnetization induced by non-thermalized hot-electrons (without Pt(10)), the
77 characteristic demagnetization times are much longer. We attributed such temporal elongation
78 to the temporal stretching of the thermalized hot-electrons pulse.

79 In this work, we investigate the changes induced by the insertion of a ferromagnetic
80 [Co(0.1)/Ni(0.6)]_{x5} multilayer on the transport properties of hot-electron pulses. In particular,
81 we are interested in the temporal stretching and delays of the hot-electron pulses. In order to
82 describe these modifications, we have investigated the hot-electron induced demagnetization
83 in a ferrimagnetic Co₈₀Dy₂₀ alloy by means of time-resolved X-ray Magnetic Circular
84 Dichroism (tr-XMCD) [36]. We have considered the characteristic demagnetization times of
85 both Co and Dy sub-lattices to evidence the temporal stretching of the hot-electron pulses and
86 the demagnetization onsets to evidence the temporal delay of the hot-electron pulses as
87 described in our previous work [14]. We show that the insertion of a [Co(0.1)/Ni(0.6)]_{x5}
88 (thickness ~3.5 nm) multilayer results in a huge increase of the characteristic demagnetization
89 time in both the Co 3d and Dy 4f sublattices, as well as a sizable delay of the demagnetization
90 onset. These observations demonstrate that a [Co(0.1)/Ni(0.6)]_{x5} multilayer is capable of
91 efficiently thermalizing the hot-electron pulse before it acts on the CoDy layer.

92

93 **2. Material and methods**

94

95 The 18 nm thick Co₈₀Dy₂₀ (label CoDy in the text for commodity) alloys were deposited by
96 DC-magnetron sputtering on SiN membranes and capped with (sample 1) Al(5)/Ta(3),
97 (sample 2) Al(5)/Ta(3)/Cu(60)/[Co(0.1)/Ni(0.6)]_{x5}/Cu(3.5) and (sample 3)
98 Al(5)/Ta(3)/Cu(50)/Pt(9)/ [Co(0.1)/Ni(0.6)]_{x5}/Cu(3.5) multilayers (units in nm). The samples
99 are sketched in figure 1. The choice of the specific materials used as capping layers for
100 samples 2 and 3 (Al(5)/Ta(3)/Cu(X)) ensures negligible direct excitation of CoDy alloys by

101 IR pump pulses [13, 14] and guarantees at least 15% X-ray transmission at the specific CoL₃
102 and DyM₅ absorption edges. In sample 2 and 3, the hot-electron pulses are generated by IR
103 absorption in the Al(5)/Ta(3)/Cu(X) capping layers [13]. The [Co(0.1)/Ni(0.6)]_{x5} multilayer is
104 the inserted thin magnetic layer. The choice for this material was motivated by its large spin-
105 polarization at the Fermi level [35] which makes it a good candidate for future ultrafast
106 spintronic application. In sample 3, the 9 nm Pt film grown in between the 50nm Cu film and
107 the [Co(0.1)/Ni(0.6)]_{x5} multilayers acts as a barrier for the ballistic hot-electrons [14, 17]. **It**
108 **ensures that the demagnetization is caused by thermalized spin-polarized hot-electrons**
109 **in sample 3 [14]. By comparing the hot-electron induced demagnetization in sample 2**
110 **and 3, we will be able to determine if the demagnetization is caused by non-thermalized**
111 **or by thermalized spin-polarized hot-electrons in sample 2 [14].** The thin Cu(3.5) layer
112 which is grown in between **the** [Co(0.1)/Ni(0.6)]_{x5} multilayers and the buried ferrimagnetic
113 Co₈₀Dy₂₀ alloy ensures the decoupling between these magnetic layers. We have chosen CoDy
114 alloys instead of the Co₇₄Tb₂₆ alloys we have previously investigated [14] because they allow
115 investigating the hot-electron induced demagnetization of both the Co 3d “itinerant” and Dy
116 4f “localized” magnetic moment by tr-XMCD. Indeed, the XMCD amplitude at the Co L₃
117 edge of the Co₇₄Tb₂₆ alloys does not match the requirements to perform high quality tr-
118 XMCD at the femtoslicing facility, especially for limited demagnetization amplitudes as those
119 reported in this work (table 1). Furthermore, we have already investigated the direct laser
120 induced demagnetization in CoDy alloys by means of element- and time-resolved XMCD
121 experiments [37]. Therefore, the specificities of the laser and hot-electrons induced ultrafast
122 magnetization dynamics can be easily compared.

123 The time-resolved XMCD experiments were carried out at the femtoslicing beam line of the
124 BESSY II synchrotron radiation source at the Helmholtz-Zentrum Berlin [36]. We have used
125 the very same configuration for the pump-probe experiments as in a recently published work
126 [14]. The magnetization dynamics have been recorded by monitoring the transmission of
127 circularly polarized X-rays pulses tuned to specific core level absorption edges as a function
128 of a pump-probe delay for two opposite directions of the magnetic field. The photon energy
129 was set to the CoL₃ and the DyM₅ edges using the reflection zone plate monochromator at
130 UE56/1-ZPM. The experimental chamber allowed for mounting two samples, hence, we
131 measured successively samples 1 (direct pumping by IR pulses) and sample 2 or sample 3
132 (indirect excitation). We determined the temporal and spatial overlap between pump and
133 probe on sample 1 and thus determined accurately the delay induced by the thick capping
134 layers in case of indirect excitation. A 500 μm beam diameter for pump laser was selected in

135 order to ensure homogeneous pumping over the probed area of the sample (200 μm). The
 136 fluences of the laser were set to 7 mJ/cm^2 for sample 1 and 14 mJ/cm^2 for samples 2 and 3. A
 137 magnetic field of 0.55 T, sufficient to saturate both the $[\text{Co}(0.1)/\text{Ni}(0.6)]_{\text{x}5}$ multilayer and the
 138 CoDy alloys, was applied along the propagation axis of both the IR laser and the X-ray beam
 139 during the experiment. Thus, the magnetization directions of both magnetic layers are parallel
 140 in our experiment. The temperature of the cryostat was set to 280K to compensate a weak
 141 DC-heating for the samples 2 and 3 ($\sim 20\text{K}$) and ensuring an equilibrium temperature of
 142 $\sim 300\text{K}$ at negative delays. Thus the experiments were carried out above the temperature of
 143 magnetic compensation of the CoDy alloys ($T_{\text{comp}} \sim 220 \text{K}$) [37]. The total amount of Co
 144 introduced by the $[\text{Co}(0.1)/\text{Ni}(0.6)]_{\text{x}5}$ multilayers is equivalent to $\sim 0.5 \text{nm}$. This thickness is
 145 negligible compared with the Co studied in the buried ferromagnetic $\text{Co}_{80}\text{Dy}_{20}$ alloy ($\sim 14\text{nm}$).
 146 Therefore, the contribution of the $[\text{Co}(0.1)/\text{Ni}(0.6)]_{\text{x}5}$ multilayers to the XMCD signal at the
 147 Co L_3 edge can be neglected as will be shown.

148

149 **3. Results and discussions**

150

151 The transient XMCD recorded for samples 1, 2 and 3 at the Co L_3 and Dy M_5 edges are
 152 displayed in figure 2. The experimental data were fitted with two exponential functions
 153 (respectively the demagnetization and the magnetization recovery) convoluted by a Gaussian
 154 function which accounts for the experimental time resolution (130 fs) [38, 39]. The
 155 demagnetization amplitude (q), the demagnetization onset (t_0) and the characteristic
 156 demagnetization time (τ) for both Co and Dy sublattices, as well as their error bars extracted
 157 from the fits are summarized in table 1. The latter correspond to the standard deviation of
 158 experimental data with respect to the fitting function.

159

160 *Table 1: Parameters extracted from the fit functions for the 3 samples and for both Co and*
 161 *Dy.*

	Demagnetization amplitude q (%)	Demagnetization onset t_0 (ps)	Characteristic demagnetization time τ (ps)
Sample 1 Co	51 ± 5	0 ± 0.1	0.16 ± 0.03
Sample 1 Dy	98 ± 5	0 ± 0.1	0.44 ± 0.08
Sample 2 Co	16 ± 3	0.47 ± 0.15	0.33 ± 0.18

Sample 2 Dy	21 ± 3	0.45 ± 0.25	1.95 ± 0.4
Sample 3 Co	9 ± 3	1.1 ± 0.2	0.33 ± 0.2
Sample 3 Dy	19 ± 4	0.9 ± 0.35	2.25 ± 0.6

162

163 **In** sample 1, the demagnetization for both Co and Dy sublattices is driven by direct photon
164 excitations. **We observed a demagnetization amplitude $q = 98 \pm 5 \%$ and a characteristic**
165 **demagnetization times $\tau = 0.44 \pm 0.08$ ps for the Dy 4f sublattice. These values are**
166 **respectively larger and longer compared to those reported for the Co 3d sublattice ($q =$**
167 **$51 \pm 5 \%$ and $\tau = 0.16 \pm 0.03$ ps). The distinct ultrafast fs-laser induced demagnetization of**
168 **the TM and the RE sublattices have been reported in various** element- and time-resolved
169 XMCD experiments on rare-earth / transition metals alloys [37, 39 - 44]. Even if the
170 discussion of such differences is beyond the scope of this publication, several **explanations**
171 **are proposed in the literature. It may originate from the element-specific dependence of**
172 **magnetization on temperature in each sublattice [45, 46] as shown by Hofherr et al [47].**
173 **It could also arise from heat transfer from the TM sublattice towards the RE sublattice**
174 **[48]. Gort et al. have demonstrated that the characteristic demagnetization times depend**
175 **on the electron binding energy [49] while Radu et al. have established a linear relation**
176 **between τ and the magnetic moments [43].** Anyway, the measurements in sample 1 are used
177 in this study as the references for q , t_0 and τ .

178

179 In samples 2 and 3, the demagnetization is caused by the photo-excited hot-electron pulses [5,
180 13, 14]. Similar to direct IR laser excitation, the hot-electron induced demagnetization of the
181 Co 3d and the Dy 4f sublattices occurs on different time scales in spite of the Co-Dy exchange
182 coupling. By comparing photon- (sample1) and hot-electron- (sample 2 and 3) induced
183 demagnetization, we observe less pronounced demagnetization amplitudes for both the Co
184 and Dy sublattices in the second case. This is obtained in spite of larger laser fluences, and is
185 similar to previously reported results in CoTb alloys [14]. The small demagnetization
186 amplitudes in sample 2 and 3 is partly explained by the large thickness of the $\text{Co}_{80}\text{Dy}_{20}$ alloy
187 (18 nm) compared to the hot-electron penetration depth ($\lambda_{\text{up}}=6.5$ nm for the majority spins and
188 $\lambda_{\text{down}}=1.2$ nm for the minority spins in Co [50]). We also observed delays of the
189 demagnetization onset, and much longer demagnetization times for both Co and Dy
190 sublattices. These observations are of interest here and they are discussed in the following,
191 starting with the characteristic demagnetization times.

192 Considering the results of our previous work [14], we can state here that the Pt(9) layer in
193 sample 3 is capable of efficiently thermalizing the photo-excited hot-electron pulses.
194 Therefore, the much longer demagnetization times we have observed for both Co (0.33 ps
195 instead of 0.16 ps) and Dy (2.25 ps instead of 0.44 ps) in the case of hot-electron excitation
196 are readily explained. Vodungbo et al. have investigated the hot-electron induced
197 demagnetization in Al(40)/[Co(0.4)/Pd(0.2)]_{x30} multilayer [12]. In their case, the hot-electrons
198 were also thermalized in the Al capping layer before they reach the CoPd multilayer. They
199 have reported a characteristic demagnetization time of 0.43 ps for the Co sublattice instead of
200 0.16 ps for direct laser induced demagnetization. Their observations are consistent with our
201 measurements at the Co L₃ edge. Interestingly, the characteristic demagnetization times and
202 demagnetization amplitudes measured at Co and Dy edges for samples 2 and 3 are very close,
203 in spite of the additional Pt(9) layer in sample 3. These observations are not compatible with
204 non-thermalized hot-electron induced demagnetization in sample 2 (no Pt) [10, 13, 14].
205 Indeed, in this case, the characteristic demagnetization times would have been similar to those
206 reported for laser induced demagnetization [14] which is not the case. This means that the
207 demagnetization in sample 2 is most likely induced by thermalized hot-electrons. Therefore,
208 we conclude that the thin [Co(0.1)/Ni(0.6)]_{x5} multilayer is highly efficient to thermalize the
209 hot-electrons which are generated in the Al(5)/Ta(3)/Cu(60) capping layer. This efficiency is
210 probably explained by the hot-electron scattering at the numerous Co/Ni interfaces [51].
211 The photo-excited hot-electron pulses are not only temporally stretched in the
212 [Co(0.1)/Ni(0.6)]_{x5} multilayers and Pt(9) layers but additionally the group velocity is strongly
213 reduced as suggested by the reported demagnetization onsets for sample 2 (0.47 ± 0.15 ps)
214 and sample 3 (1.1 ± 0.2 ps). These demagnetization onsets are much larger than those
215 previously reported in Pt(3)/Cu(80)/CoPt (~ 0.12 ps) [13]. Such delays are also readily
216 explained by the thermalization of the hot-electrons in the [Co(0.1)/Ni(0.6)]_{x5} multilayers.
217 The values are consistent with those we have reported previously for CoTb alloys with a
218 Pt(10) layer ($\sim 0.35 \pm 0.2$ ps) [14]. **It is worth noticing that the magnetization of the**
219 **[Co(0.1)/Ni(0.6)]_{x5} multilayer will partly be quenched by the hot-electron pulses [13].**
220 **This demagnetization will affect the spin-polarization of the hot-electron pulses [10, 22,**
221 **23] and** should occur at $t_0 \sim 0.1$ ps [13]. We do not observe the demagnetization of the
222 [Co(0.1)/Ni(0.6)]_{x5} multilayers because the signal to noise ratio does not allow to resolve the
223 dynamics of such an ultrathin magnetic layer. **Therefore, the longer demagnetization onsets**
224 **we have reported here** confirm that the transient XMCD signals at the Co L₃ edges measured
225 for sample 2 and 3 (figure 2) are solely defining the ultrafast dynamics in the CoDy alloys.

226

227 We show that the $[\text{Co}(0.1)/\text{Ni}(0.6)]_{x5}$ multilayer results in a temporal stretching and a delay of
228 the hot-electron pulses. Therefore, our results suggest that by engineering thin magnetic layers
229 with suitable properties, one can tune the pulse duration of spin-polarized hot-electrons. For
230 instance, recent studies have shown that a longer spin-polarized hot-electron pulse could be
231 more efficient at inducing ultrafast magnetization switching [33, 52]. In this light, our results
232 pave the way to more controlled and efficient magnetization switching.

233

234 *4. Conclusions*

235

236 We have reported on the hot-electron induced demagnetization in $\text{Co}_{80}\text{Dy}_{20}$ alloys by element-
237 and time-resolved XMCD. We observed disparate dynamics in terms **of demagnetization**
238 **times for Co 3d and for Dy 4f sublattices similar to direct laser induced demagnetization.**
239 We have shown that inserting a $[\text{Co}(0.1)/\text{Ni}(0.6)]_{x5}$ multilayer results in a temporal stretching
240 of the photo-excited hot-electron pulses and a reduction of its group velocity. **These tailored**
241 **SP hot-electron pulses offer prospects for more efficient ultrafast magnetization**
242 **switching.** This study calls for more systematic experimental and theoretical investigations in
243 order to determine the spin-polarization of the hot-electrons pulses **and how it is affected by**
244 **the demagnetization of the $[\text{Co}(0.1)/\text{Ni}(0.6)]_{x5}$ multilayer.**

245

246 *References:*

247

- 248 [1]: Beaurepaire et al. Phys. Rev. Lett., 76, 4250 (1996)
249 [2]: Kirilyuk et al. Rev. Mod. Phys., 82, 2731 (2010)
250 [3]: Kirilyuk et al. Rep. Prog. Phys. 76, 026501 (2013)
251 [4]: Bigot et al. Ann. Phys. 1, 2 (2013)
252 [5]: Malinowski et al. Eur. Phys. J. B. 91, 98 (2018)
253 [6]: Stanciu et al. Phys. Rev. Lett. 99, 047601 (2007)
254 [7]: Ostler et al. Nature Commun. 3, 666 (2012)
255 [8]: El Hadri et al. Phys. Rev. B 94, 064412 (2016)
256 [9]: Laliou et al. Phys. Rev. B 96, 220411(R) (2017)
257 [10]: Eschenlohr et al. Nature Mater. 12, 332 (2013)
258 [11]: Salvatella, Structural Dynamics 3, 055101 (2016)

259 [12]: Vodungbo et al. Scientific Reports 6, 18970 (2016)
260 [13]: Berggaard et al. Phys. Rev. Lett. 117, 147203 (2016)
261 [14]: Ferté et al. Phys. Rev. B 96, 144427 (2017)
262 [15]: Xu et al. Advanced Materials (2017)
263 [16]: Schellekens et al. Nature Communications 5, 4333 (2014)
264 [17]: Choi et al. Nature Communications 5, 4334 (2014)
265 [18]: Choi et al. Nature Physics 11, 576 (2015)
266 [19]: Razdolski et al. J. of Phys. Condens. Matt. 29, 174002 (2017)
267 [20]: Alekhin et al. Phys. Rev. Lett. 119, 017202 (2017)
268 [21]: Baláž et al. J. Phys.: Condens. Matter. 30, 115801 (2018)
269 [22]: Battiato et al. Phys. Rev. Lett. 105, 027203 (2010)
270 [23]: Battiato et al. Phys. Rev. B 86, 024404 (2012)
271 [24]: Malinowski et al. Nature Physics 4, 855 (2008)
272 [25]: Melnikov et al. Phys. Rev. Lett. 107, 076601 (2011)
273 [26]: Turgut et al. Phys. Rev. Lett. 110, 197201 (2013)
274 [27]: Wieczorek et al. Phys. Rev. B 92, 174410 (2015)
275 [28]: Chen et al. Appl. Phys. Lett. 110, 092407 (2017)
276 [29]: Shokeen et al. Phys. Rev. Lett. 119, 107203 (2017)
277 [30]: Khorsand et al. Nature Matter. 13, 101 (2014)
278 [31]: Brorson et al. Phys. Rev. Lett. 59, 1962 (1987)
279 [32]: Juhasz et al. Phys. Rev. B 48, 15488 (1993)
280 [33]: Iihama et al. Advanced Materials. 30, 1804004 (2018)
281 [34]: Stiles Journal of Appl. Phys. **79**, 5805 (1996)
282 [35]: Ueda et al. Appl. Phys. Lett. 100, 202407 (2012)
283 [36]: Holldack et al. J. Synchrotron Rad. 21, 1090 (2014)
284 [37]: Ferté et al. Phys. Rev. B 96, 134303 (2017)
285 [38]: Boeglin et al. Nature 465, 458 (2010)
286 [39]: Berggaard et al. Nature Communications 5, 3466 (2014)
287 [40]: Radu et al, Nature. 472, 205 (2011)
288 [41]: Lopez-Flores et al. Phys. Rev. B 87, 214412 (2013)
289 [42]: Graves et al. Nature Materials. 12, 293 (2013)
290 [43]: Radu et al. SPIN, 5, 1550004 (2015)
291 [44]: Higley et al. Rev. of Sci. Instrum. 87, 033110 (2016)
292 **[45]: Chen et al. Phys. Rev. B 91, 024409 (2015)**

293 [46]: Donges et al. Phys. Rev. B 96, 024412 (2017)
 294 [47]: Hofherr et al. Phys. Rev. B 98, 174419 (2018)
 295 [48]: Mekonnen et al. Phys. Rev. B 87, 180406(R) (2013)
 296 [49]: Gort et al. Phys. Rev. Lett. 121, 087206 (2018)
 297 [50] Dijken et al. Phys. Rev. B 66, 094417 (2002)
 298 [51]: Choi et al. Phys. Rev. B. 89, 064307 (2014)
 299 [52]: Choi et al. Phys. Rev. B 97, 014410 (2018)

300

301 **Acknowledgments:**

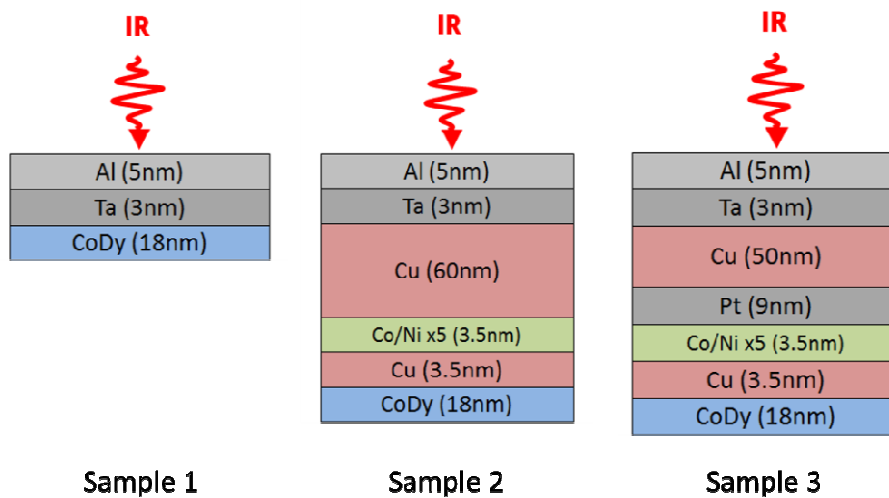
302 We are indebted for the scientific and technical support given by N. Pontius, Ch. Schüßler-
 303 Langeheine and R. Mitzner at the slicing facility at the BESSY II storage ring. The authors
 304 are grateful for financial support received from the following agencies: the French “Agence
 305 National de la Recherche” via Project No. ANR-11-LABX-0058_NIE and Project EQUIPEX
 306 UNION No. ANR-10-EQPX-52, the CNRS-PICS program, the EU Contract Integrated
 307 Infrastructure Initiative I3 in FP6 Project No.R II 3CT-2004-50600008. Experiments were
 308 carried out on the IJL Project TUBE-Davms equipment funded by FEDER (EU), PIA
 309 (Programme Investissemnet d’Avenir), Region Grand Est, Metropole Grand Nancy, and
 310 ICEEL.

311

312 The authors have no competing interests to declare

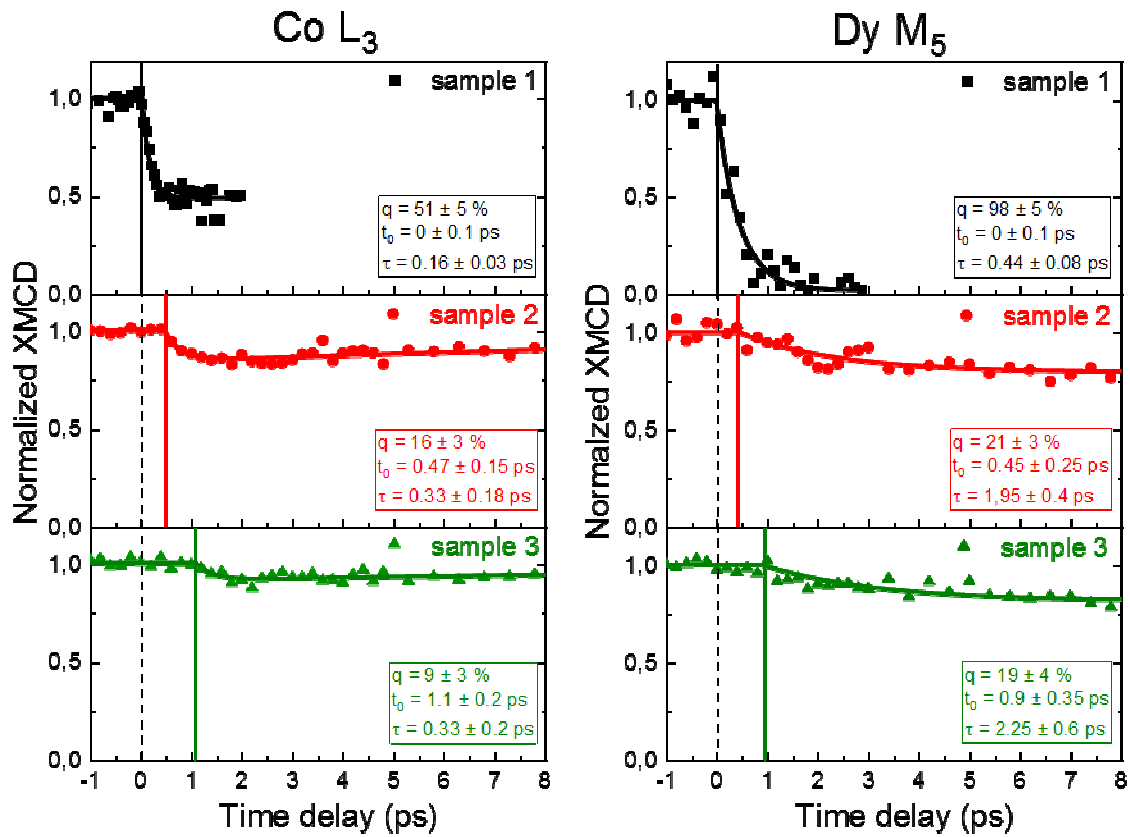
313

314 **Figures:**



315

316 *Figure 1: Sketches of the layer structures of the different samples and the geometry of laser excitation (IR, perpendicular to*
 317 *the surface normal).*



319

320 *Figure 2: Transient XMCD as a function of the pump-probe delay at the Co L₃ (left column) and Dy M₅ (right column) for*
 321 *sample 1 (black squares), 2 (red circles) and 3 (green triangles) and the corresponding single exponential fits (thick lines). The*
 322 *demagnetization onsets determined from the fits are indicated by the thin vertical lines.*

323

324

325

326

327

328

329

330

331

332

333

334

335

336